Morphological evolution of growing crystals: A Monte Carlo simulation

Rong-Fu Xiao, J. Iwan D. Alexander, and Franz Rosenberger
Center for Microgravity and Materials Research, University of Alabama in Huntsville, Huntsville, Alabama 35899
(Received 10 March 1988)

A Monte Carlo model is used to simulate the morphological evolution of crystals growing from a vapor phase. The model combines nutrient diffusion, based on a modified diffusion-limited aggregation (DLA) process, with anisotropic surface-attachment kinetics and surface diffusion. First- and second-nearest-neighbor interactions are taken into account. Through a systematic variation of the simulation (growth) parameters, the whole range of growth morphologies observed in nature is recovered. Depending on the imposed temperature, supersaturation, and bond energies, the model crystals are found to grow either fully faceted or with (dendritic) protrusions which, in turn, can either be branchless or develop side branches with smooth or split tips. The successive transitions from compact faceted to open dendritic morphologies are seen to arise as a collective result of nutrient diffusion and interface kinetics. The scale invariance exhibited by DLA does not generally hold in (dendritic) crystal growth. Thus, this work is not only an extension of previous DLA-type simulations, but affords physical insight into the nature of the interaction of crystal morphology with surface and volume processes.

I. INTRODUCTION AND BACKGROUND

The growth morphology and morphological stability of a crystal is an extremely complex problem, involving, in general, an interaction between the effects of nutrient diffusion and surface kinetics.[1-8] The wide variety of naturally occuring crystal morphologies attests to this complexity. Owing to the nonequilibrium conditions that necessarily prevail during the growth of crystals, the traditional theories[9-14] dealing with the equilibrium (minimum-free-energy) shapes of crystals are often inapplicable.

Two basic approaches to the morphological description of crystal growth have been adopted. The first is the macroscopic approach which involves the solution of a continuum diffusion equation coupled with moving boundary conditions.[15,16] The second is the simulation of microscopic processes by tracking the individual growth units (particles). The tracking of individual growth units is commonly dealt with using a Monte Carlo (MC) method.[17] Such simulations have widely been used to study the dependence of surface roughening, surface melting, and growth rate on supersaturation and temperature.[18-20] These studies were primarily focused on interfacial kinetics and have occasionally included surface diffusion.[21] The influence of nutrient diffusion, i.e., the transport of growth units to the interface and dissipation of latent heat, have received less attention. In the event that surface diffusion and interfacial kinetics govern the growth morphology, these simplifications are not a severe limitation. However, in reality, nutrient bulk diffusion often plays the decisive role in limiting morphological stability.[8,16,22]

The recently developed diffusion-limited aggregation (DLA) model of Witten and Sander[23,24] would seem particularly appropriate to describe nutrient diffusion in crystal growth. The DLA model simulates the growth of an aggregate by considering the random walk of a particle on a lattice containing a seed. If the mobile particle encounters the seed, it ceases to move. As successive walkers repeat this process, aggregates are produced of which Fig. 1(a) is a typical example. By introducing a sticking probability of less than one, several workers[24,25] have shown that the morphology of these aggregates can be modified. Rather than allowing the moving particle to simply become part of the aggregate upon arrival at an unoccupied interfacial (growth) site, the probability P_i that a particle will adhere at an interfacial position is calculated based on nearest-neighbor considerations. For example, for a triangular lattice, P_i could have the form

$$P_i = t^{5-n_i} , \tag{1}$$

where t is the sticking coefficient and n_i is the number of occupied nearest neighbors. Thus, the probability that a particle will attach to a growth site increases with the number of nearest neighbors of that site. Figure 1(b) presents a typical growth pattern obtained using (1) with $t=0.6$ and otherwise identical simulation conditions to those of Fig. 1(a). Note that while the aggregate retains the essential features of Fig. 1(a), the lower value of t results in a more compact figure.

Witten and Sander[24] proposed that the more compact form results because a sticking coefficient of less than one corresponds to a Gibbs-Thomson effect, while a value of unity corresponds to zero surface tension. However, a boundary condition of the form (1) is a local statement and contains no information regarding the curvature of the interface. Condition (1), simply owing to its bias towards growth sites with a greater number of nearest neighbors, will result in a more compact figure. This has the flavor of a Gibbs-Thomson effect. However, as shown by Fig. 1(b), the short-range nature of (1) cannot lead to the elimination of short-wavelength disturbances

characteristic of realistically scaled capillarity.

A more realistic account of capillarity was introduced by Vicsek.[26,27] He replaced (1) with a Gibbs-Thomson relation based on an approximate local curvature. In addition, Vicsek allowed particles that attach to the surface to diffuse towards a site with higher number of nearest neighbors. In this way, dendritelike shapes were obtained. At some intermediate scale the growth shapes obtained by Vicsek reflect the stabilizing effect of capillarity. However, the short-wavelength noise similar to that exhibited in Fig. 1(b) is still present.

A MC simulation of the site-occupation probability should be the average of many independent walks to a given growth site. Consider N independent walks; if an event has a probability q of occuring, then the fraction of outcomes A approaches q as $N \rightarrow \infty$. By choosing N to be large enough, the average outcome of the N-independent walks will differ from the expected value by a small amount. In principle, this can be realized by implementing the following averaging scheme: rather than take a single walk as an independent contribution to the growth of the aggregate, a multiple registration for every interfacial site is considered. The interfacial site can be occupied only when it has been registered N times. After occupation, the previous registration for all interfacial sites is reset to zero and new registration along the whole interface resumes. However, the above averaging scheme is impractical because of computational time limitation. To remedy this problem, Tang[28] introduced a quasiaveraging scheme which ignored the procedure of resetting every interfacial site to zero after one occupation. While this is not a rigorous averaging scheme it results in a significant reduction of spatial noise. Applying Tang's idea, Nittmann and Stanley[29] and Ball[30] obtained snowflakelike patterns.

In this work we used a MC method to simulate the evolving morphology of a growing crystal by considering random walks of particles on a two-dimensional (2D) triangular lattice. While previous DLA models have based their formulation of boundary conditions on loosely drawn analogies with continuum descriptions of crystal growth, we based our boundary conditions on explicit considerations of microscopic crystal-growth kinetics. This formulation of nutrient diffusion and interfacial kinetics of the growth processes is presented in Sec. II. Section III is a brief description of the simulation procedure. The results are presented and discussed in Sec. IV.

II. MODEL AND FORMULATION

During crystal growth, an individual growth unit usually undergoes two basic processes before becoming part of the growing crystal. After having left the source reservoir, the growth unit is transported towards the interface via diffusion and convection in the nutrient. Second, when the particle reaches the crystal surface, it does not, in general, become immediately incorporated into the growing crystal, but wanders about the interface in an attempt to find an energetically favorable growth site. During this period the growth unit will interact with the particles already on the interface, and the final attachment of the growth unit is controlled by interfacial kinetics.[31] Owing to the intrinsic anisotropic nature of the crystal lattice, the attachment of the growth unit will inevitably reflect the crystalline anisotropy. Thus, in contrast to models of the growth of isotropic aggregates,[32] any realistic description of crystal growth must, in general, take anisotropic surface kinetics into account. In the following sections we discuss the formulation of a Monte Carlo (MC) model of crystal growth from a vapor which considers both nutrient diffusion and surface kinetics.

A. Mass diffusion in the nutrient

We assume that the motion and aggregation of growth units take place on a 2D grid, and restrict our study to a physical system with the following properties: (1) The nutrient phase is gaseous. (2) The nutrient phase consists of two components. Component A, the growth species, is highly diluted in an inert gas B, which randomizes the motion of A. (3) The total vapor pressure ($p = p_A + p_B$) is constant. (4) There is no convective motion of the nutrient. Mass transfer occurs only by diffusion. (5) The system is isothermal, i.e., heat conduction is rapid compared to mass diffusion. Thus, the latent heat released during crystallization can be ignored.

These assumptions are consistent with the following Monte Carlo model. The motion of a given growth unit is described by a simple random walk, and the jump lengths of the random walk are equal everywhere. The probability $U(\mathbf{r}, k\tau)$ that a particle can be found at location $\mathbf{r}$ after k steps is taken to be

$$U(\mathbf{r}, k\tau) = \frac{1}{c} \sum_{\mathbf{a}} U[\mathbf{r}+\mathbf{a}, (k-1), \tau] , \tag{2}$$

where $c=6$ for a triangular grid, τ is the time needed for one single jump, and $\mathbf{a}$ represents the six possible jump directions. Equation (2) is a discretized version of the diffusion equation[24,33]

$$\frac{\partial U}{\partial t} = D \nabla^2 U . \tag{3}$$

For the case of mass diffusion the probability $U(\mathbf{r}, t)$ can be considered as a normalized concentration

$$U(\mathbf{r}, t) = \frac{C(\mathbf{r}, t)}{C_{\max}} , \tag{4}$$

where $C_{\max}$ is the concentration at the source. Clearly, from Eq. (4) the boundary condition at the source is $U \equiv 1$, i.e., in a given simulation the source is maintained at a fixed concentration.

B. Surface kinetics

When the growth unit reaches the crystal surface, it will either stick to the surface, adsorb and diffuse on the surface, or even return to the nutrient after a (short) residence time on the interface. The latter happens, for instance, when the growth unit is misoriented and cannot form stable bonds with the crystal. Alternatively, the growth unit may impinge onto a site with too-few neigh-

bors to prevent it from being dislodged by thermal vibrations. To describe such complicated processes, we assume that the probability that a particle will stick onto the surface can be calculated from a consideration of the impingement and evaporation rate, and the probability that the particle undergoes surface diffusion can be obtained from the occupation conditions about its nearest and next-nearest neighbors.

The impingement rate is closely related to the mass flux or the concentration gradient in the nutrient near the interface. In vapor crystal growth, the rate K^+ of particles impinging onto a surface, is, according to the kinetic theory of gases, proportional to the interfacial vapor pressure p_A of the growth species and is given by

$$K^+ = p_A/(2\pi mkT)^{1/2} , \tag{5}$$

where k, m, and T are, respectively, the Boltzmann constant, mass of the growth unit, and the absolute temperature of the system.

As a first approximation we assume that we may take K^+ to be dependent on the average vapor pressure $\bar{p}_A$ rather than p_A (the actual local configuration-dependent vapor pressure at the crystal surface). The implications of this assumption will be discussed further in Sec. IV. Then, consistent with our assumptions (1), (2), and (5), the following relation can be applied:[34]

$$\Delta\bar{G} = RT\ln(\bar{p}_A/p_{A0}) , \tag{6}$$

where $\Delta\bar{G} = G_v - G_{eq}$ is the average Gibbs-free-energy difference at constant temperature in the supersaturated vapor with respect to bulk equilibrium, and p_{A0} is the equilibrium value of $\bar{p}_A$.

A combination of Eqs. (5) and (6) yields

$$K^+ = K_{eq}\exp(\Delta\mu/kT) , \tag{7}$$

where K_{eq} is the temperature-dependent equilibrium value of K^+, and $\Delta\mu = \Delta\bar{G}/N_0$ with Avogadro's constant N_0 is the bulk average chemical potential difference per particle in the vapor.

The evaporation rate K_i^- is highly sensitive to the local configuration of the surface of the growing crystal. To escape from the crystal surface, the molecule must break all bonds with its solid neighbors. In general, the K_i^- can be expressed as[21,31]

$$K_i^- = \nu\exp(-E_i/kT) , \tag{8}$$

where ν is a vibration factor and E_i is the interaction energy between the growth unit and its solid neighbors. If only nearest- and next-nearest-neighbor interactions on a triangular lattice are considered, E_i can be expressed as

$$\begin{aligned} E_i &= \phi_1 \sum_{j=1}^{5} S_i S_j + \phi_2 \sum_{r=1}^{11} S_i S_r , \\ &= \phi_1(n_i + \zeta m_i) , \end{aligned} \tag{9}$$

where S_k takes on the value 1 for an occupied site and 0 for an unoccupied site, n_i and m_i are the number of occupied nearest and next-nearest neighbors of site i, respectively; ϕ_1 and ϕ_2 are the interaction energies of a molecule with its nearest and next-nearest neighbors. The ratio $\zeta = \phi_2/\phi_1$ can be zero, positive, or negative depending on whether the next-neighbor interaction is negligible, attractive, or repulsive. In reality, $\zeta \simeq 0$ holds only in the case of short-range interaction such as molecular crystals in which the bonding energy obeys a Lennard-Jones potential. For most other materials the next-nearest-neighbor interaction cannot be ignored (i.e., $\zeta \neq 0$).

The probability that a growth unit sticks onto the crystal surface is then

$$P_i = \frac{K^+}{K^+ + K_i^-} = \frac{K_{eq}\exp(\Delta\mu/kT)}{K_{eq}\exp(\Delta\mu/kT) + \nu\exp(-E_i/kT)} . \tag{10}$$

In order to relate K_{eq} and ν we assume local equilibrium at the interface and equate the rates of impingement and evaporation. For a triangular lattice this yields

$$K_{eq} = \nu\exp\left[-\frac{\phi_1}{kT}(3+6\zeta)\right] . \tag{11}$$

Then, we obtain

$$P_i = \frac{\gamma\beta^{(3-n_i)+\zeta(6-m_i)}}{1+\gamma\beta^{(3-n_i)+\zeta(6-m_i)}} , \tag{12}$$

where $\gamma = \exp(\Delta\mu/kT)$ and $\beta = \exp(-\phi_1/kT)$. It should be realized that the crystal anisotropy has been taken into account implicitly in (12), simply because of the different n_i and m_i along different orientations.

If the impinging molecule does not stay at its initial impingement site, it may either undergo surface diffusion or return to the nutrient. To account for these possibilities we consider the rate at which the particle will diffuse along the surface. This will depend on the occupation condition of the nearest and next-nearest sites to both the site i that the particle occupies and the potential jump site j. Hence, we express the jump rate as

$$K_{i\to j} = \nu_s\exp(-\Delta E_{ji}/kT) , \tag{13}$$

where the activation energy

$$\Delta E_{ji} \simeq \phi_1[(n_i - n_j) + \zeta(m_i - m_j)] ,$$

n and m refer to the number of nearest and next-nearest neighbors, with indices i and j designating the initial and final site of a jump process.

The jump probability from site i to a neighboring unoccupied site j (on the surface or in the nutrient) is then

$$P_{i\to j} = \frac{K_{i\to j}}{\sum_{j=1}^{c'} K_{i\to j}} = \frac{\beta^{(n_i-n_j)+\zeta(m_i-m_j)}}{\sum_{j=1}^{c'} \beta^{(n_i-n_j)+\zeta(m_i-m_j)}} , \tag{14}$$

where c' is the number of unoccupied nearest neighbors of site i. Clearly, larger n_j and m_j result in a higher probability that a molecule will jump to site j on the interface. The combination of (12) and (14) contains the essential physics of surface kinetics for a crystal growing from the vapor. Note, however, that in order to obtain (14) we have assumed that the vibration factor ν_s is independent of local configuration, i.e., $\nu_s^i = \nu_s^j$.

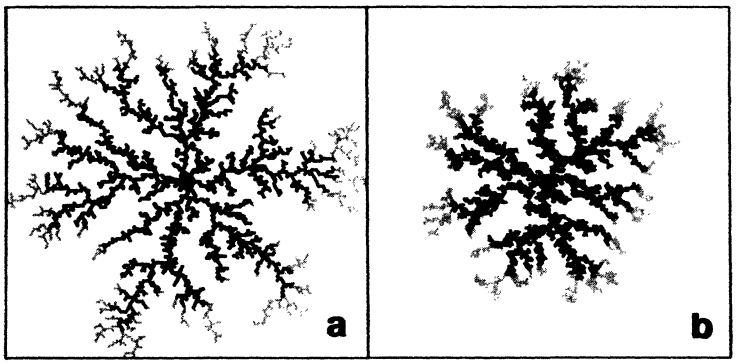

FIG. 1. Results of DLA on a 2D triangular lattice for 3×10^3 growth units. The colors represent time sequences of the growth patterns. (a) Sticking coefficient $t=1$; (b) sticking coefficient $t=0.6$.

In order to obtain a qualitative understanding of the influence of surface diffusion on crystal morphology, we consider the components of J, the total mass flux towards the interface. These are

$$J=J_1+J_2+J_3 ,$$

where J_1 is the flux of particles directly incorporating into the crystal, J_2 and J_3 are the fluxes of the particles diffusing on the interface and back to the nutrient, respectively. The following relations hold:

$$\begin{aligned} &|J_1| \sim P_i , \\ &|J_2|+|J_3| \sim (1-P_i) , \\ &|J_2|/|J_3| \sim \sum P_{i\to s} \Big/ \sum P_{i\to n} . \end{aligned} \tag{15}$$

From (15) we obtain the flux ratio $\eta=|J_2|/|J_1|$:

$$\begin{aligned} \eta &= \frac{\exp(-\Delta\mu/kT)}{W\exp\{-\phi_1[(3-n_i)+\zeta(6-m_i)]\}} , \\ &= \frac{1}{W\gamma\beta^{(3-n_i)+\zeta(6-m_i)}} , \end{aligned} \tag{16}$$

where

$$W=1+\sum P_{i\to n} \Big/ \sum P_{i\to s}$$

describes the relative weight of reevaporation and surface diffusion. From Eq. (16) we can see that the flux distribution depends on temperature, interaction energy, orientation, and supersaturation (i.e., the chemical potential difference $\Delta\mu$). As the supersaturation is increased, the ratio η decreases, i.e., surface diffusion becomes less significant relative to volume diffusion.

III. SIMULATION PROCEDURE

A summary of the steps involved in the simulation is presented in Fig. 2. The simulation takes place on a 2D triangular grid. Initially, a nucleus with radius r_0 is located at the center. A random walker is released from a "circular source" outside the central cluster, and a random walk within the nutrient ensues. We found that for triangular lattice the simulations are unaffected by the proximity of the source region to the growing crystal if the source location is $r'\geq r_{\max}+5$, where $r_{\max}$ is the radius of gyration of the growing cluster. The restriction of random walks to this "close" distance saves considerable computer time. A similar simplification was used by Meakin.[35]

The random walk is pursued until the walker encounters the interface. The nearest- and next-nearest-neighboring configurations of that site are then checked and the sticking probability P_i calculated. A random number R, $0<R\leq1$, is generated. If $R<P_i$, a registration to site i is made, and then that walker is retired. If $R>P_i$, the walker will leave the site i without registration and jump to one of its unoccupied neighboring sites. The jump probability which determines the new location

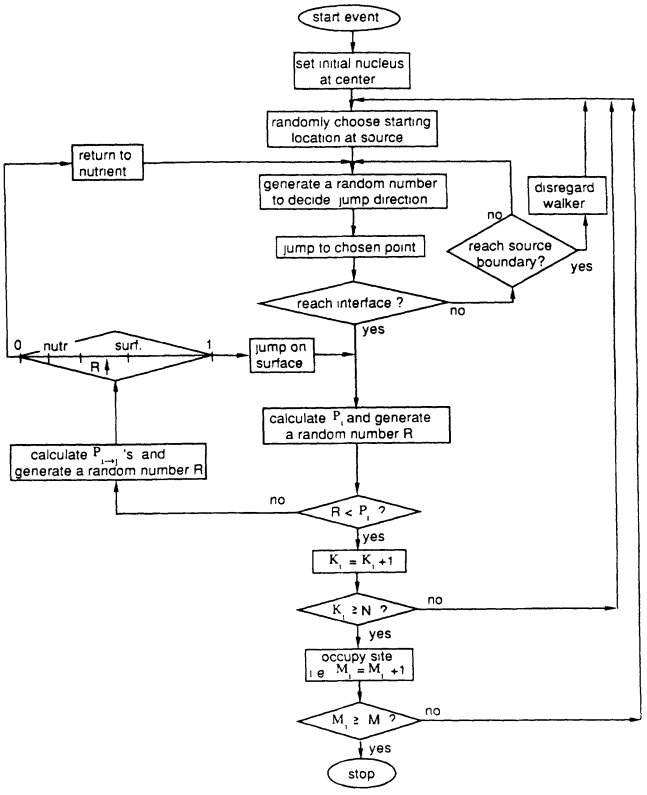

FIG. 2. Flowchart of simulation steps.

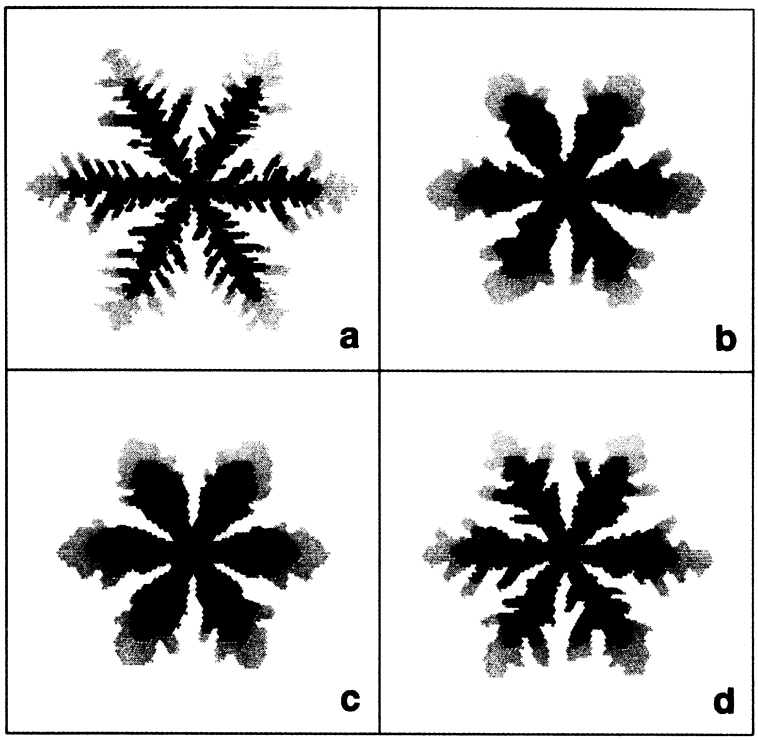

FIG. 3. Effect of surface diffusion and next-nearest-neighbor interaction on growth pattern at constant $\gamma=2$ or $\Delta\mu/kT=0.69$, and $\beta=0.6$ or $\phi_1/kT=0.51$, for 3×10^3 growth units. (a) Without surface diffusion and $\zeta=0.0$; (b) with surface diffusion and $\zeta=0.0$; (c) with surface diffusion and $\zeta=0.1$; (d) with surface diffusion and $\zeta=-0.1$.

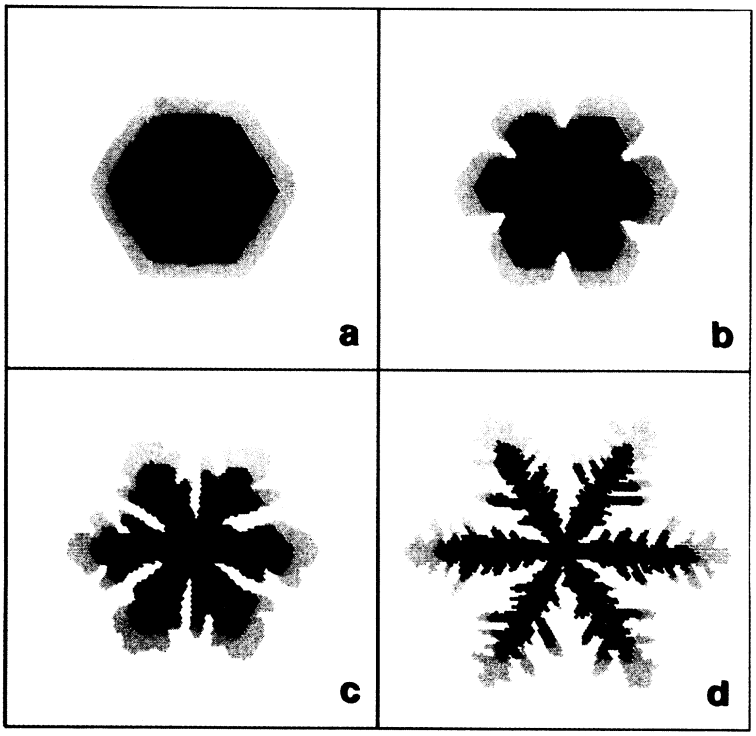

FIG. 4. Effect of bond strength and temperature on growth patterns of a crystal with surface diffusion at $\gamma=2$ or $\Delta\mu/kT=0.69$ and $\zeta=0.0$. (a) $\beta=0.02$ or $\phi_1/kT=3.91$; (b) $\beta=0.1$ or $\phi_1/kT=2.30$; (c) $\beta=0.5$ or $\phi_1/kT=0.69$; (d) $\beta=0.7$ or $\phi_1/kT=0.36$.

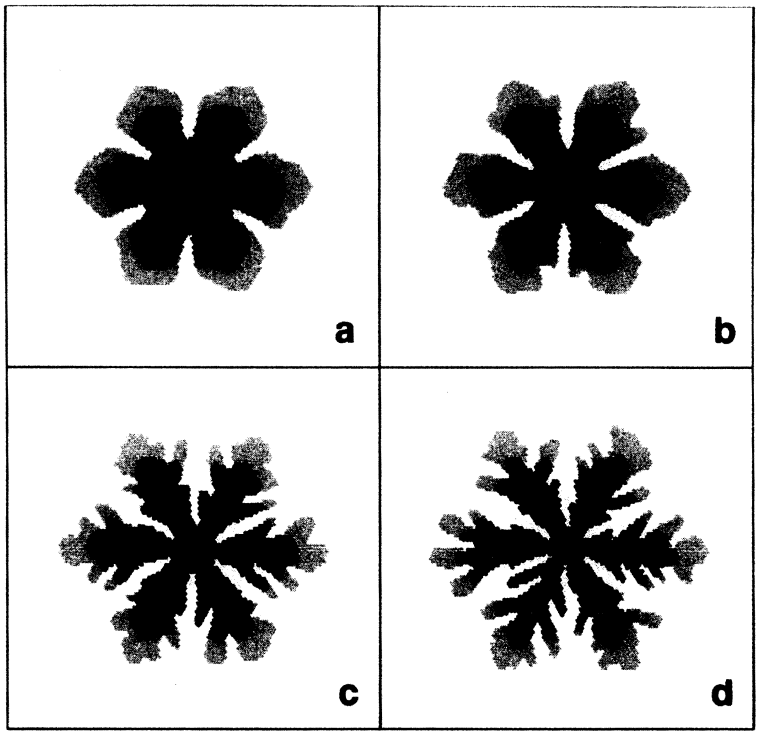

FIG. 5. Effect of supersaturation on growth patterns of a crystal with surface diffusion at $\beta=0.4$ or $\phi_1/kT=0.92$ and $\zeta=0.0$. (a) $\gamma=1.2$ or $\Delta\mu/kT=0.18$; (b) $\gamma=2.0$ or $\Delta\mu/kT=0.69$; (c) $\gamma=5.0$ or $\Delta\mu/kT=1.61$; (d) $\gamma=10.0$ or $\Delta\mu/kT=2.3$.

on the interface or in the nutrient is calculated according to (14). For typical values of the interaction parameters the probability that the particle returns to the nutrient is much less than that for continued residence on the surface. Under these conditions the walker essentially moves (or diffuses) on the interface.

As the walker jumps to a new unoccupied site i', the above procedure is resumed. Successive walkers are released from the outer source, and they proceed to undergo random motion until they either escape across the source boundary or make a registration at an interfacial site. When a site has been registered N times, it is considered to be occupied. A larger number of registrations N has the effect of reducing the noise inherent in simulation of this kind. By adopting this averaging scheme (used by Tang[28]) we find that noise is reduced significantly for $N \geq 100$. The simulation is continued until the crystal reaches a specified size.

For the parameter ranges under consideration (3×10^4 particles, $0<\gamma\leq10$, $0.001\leq\beta\leq0.8$, $N=100$) the amount of cpu time required on a VAX 785 for each simulation ranged from 2 to 10 h. To show the time sequence of the growth pattern, we subdivided the total 3×10^3 growth units into three groups. The particles in black, red, and yellow are, respectively, the first, second, and last group to arrive.

IV. RESULTS AND DISCUSSION

Figure 3 shows the effects of surface diffusion and next-nearest-neighbor interaction on the growth pattern.

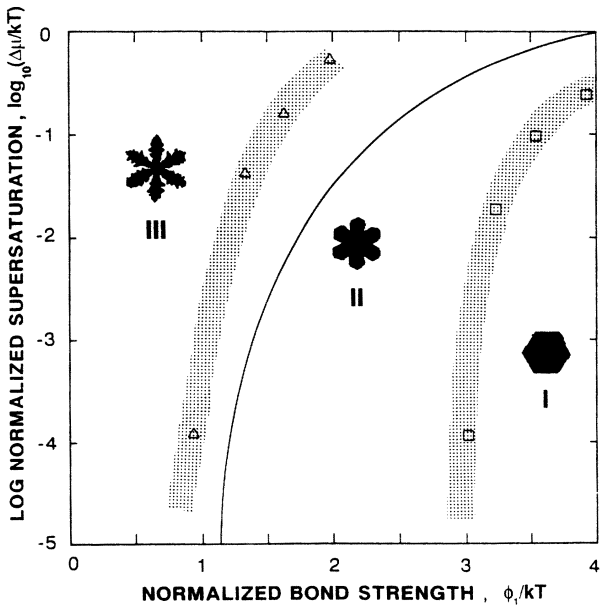

FIG. 6. Crystal-growth morphology as a collective effect of supersaturation, bond strength, and temperature. In region I crystals acquire compact-faceted forms; in region II crystals become protruded branchless needles with sixfold symmetry; in region III crystals become dendrites with multiple sidebranches. Symbols: Monte Carlo results judged as "boundary cases." Solid line: Temkin's (Ref. 36) boundary between faceted and nonfaceted growth for a simple cubic lattice.

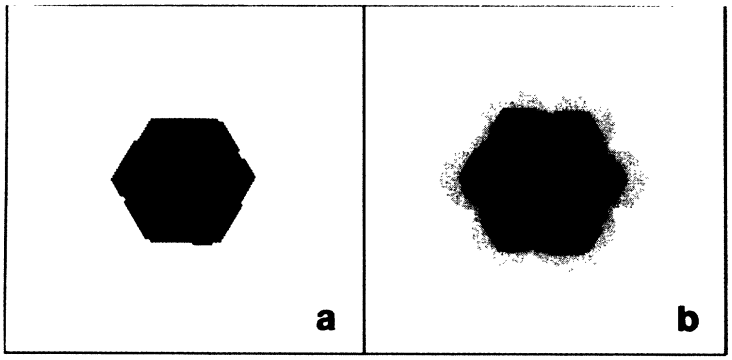

FIG. 7. Crystal size dependence of morphological stability, $\gamma=1.2$, $\beta=0.1$, $\zeta=0.1$, and with surface diffusion. (a) Crystal of 1.5×10^3 particles is still faceted; (b) facets on crystal of 3×10^3 particles lose their shape stability.

In this figure, $\gamma=\exp(\Delta\mu/kT)$ and $\beta=\exp(-\phi_1/kT)$ are kept constant and $\zeta=\phi_2/\phi_1$ is taken to be zero [Figs. 3(a) and 3(b)], positive [Fig. 3(c)], and negative [Fig. 3(d)]. Figure 3(a) was generated without and Fig. 3(b) with surface diffusion. One sees that surface diffusion helps smooth and thicken the growth pattern. Figure 3(c) clearly shows that at $\zeta=0.1$, i.e., attractive next-nearest-neighbor interaction, the branches are thicker in comparison to the shapes obtained with $\zeta=0$. In the opposite case, $\zeta=-0.1$, the pattern is more divergent [Fig. 3(d)] due to the counter effect of ϕ_2, i.e., a repulsive force exists between site i and its next-nearest neighbors.

Figure 4 shows the effect of bond strength or growth temperature, i.e., ϕ_1/kT on growth pattern for a constant value of supersaturation ($\gamma=2.0$ or $\Delta\mu/kT\simeq0.7$). One can see how the crystal morphology changes from a faceted form [Fig. 4(a)] to a branched pattern with six main protrusions [Fig. 4(b)]. Finally, at a higher value of β, it becomes akin to a "snowflake" with multiple side-branches [Figs. 4(c) and 4(d)]. An increase in β is equivalent to an increase in temperature or a decrease in the bond energy. At low temperatures, despite an appreciable supersaturation, the crystal is still able to retain a compact faceted form. Further increase of the temperature results in more open structures [see Figs. 4(c) and 4(d)].

The basic driving force for the diffusion of A towards the growing solid is the difference in chemical potential (or the supersaturation) between the crystal surface and the source region, i.e.,

$$\Delta\mu_\infty=\mu_\infty(p_{A\infty},T)-\mu_s(p_{As},T)\ . \tag{17}$$

Here p_{As} and $p_{A\infty}$ are the vapor pressure at the crystal and source. Since we have accounted for bulk nutrient diffusion via a random-walk process, $\Delta\mu_\infty$ does not appear explicitly in our model. Bulk diffusion effects do, however, arise indirectly through the assumption that the sticking probability P_i [Eq. (10)] depends on the impingement rate K^+ [Eq. (7)]. The dependence of P_i on K^+ leads, in general, to a dependence on interfacial supersaturation. The interfacial supersaturation is represented by the chemical potential difference

$$\Delta\mu_s=\mu_s(p_{As},T)-\mu_{\rm eq}(p_{A0},T)\ . \tag{18}$$

Since p_{As} will, in general, vary over the crystal surface, $\Delta\mu_s$ (and thus the interfacial supersaturation) will not be uniform. In our simulation we have assumed that p_{As} in Eq. (6) may be replaced by $\bar{p}_{As}$ (the average vapor pressure). As a result the sticking probability is independent of local variations in the supersaturation, but does depend on the average or bulk supersaturation defined by the chemical potential difference

$$\Delta\mu=\mu(\bar{p}_A,T)-\mu_{\rm eq}(p_{A0},T)\ , \tag{19}$$

as defined through Eq. (6).

We emphasize that we retain the essential effect of in-

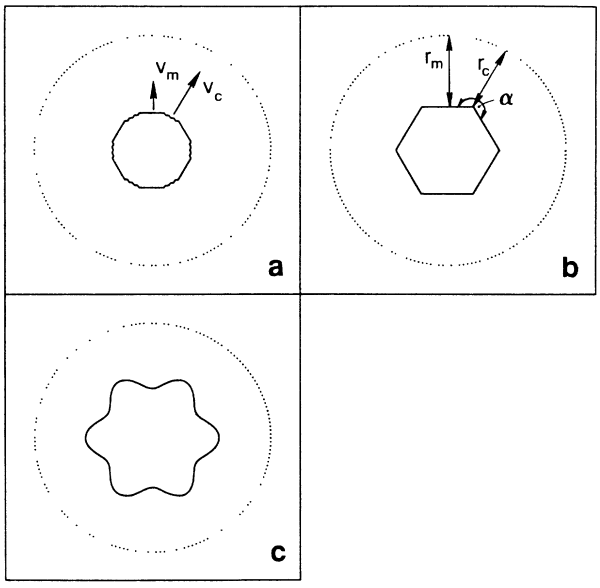

FIG. 8. Schematic illustration of formation of a dendritic crystal. (a) Initially circular nucleus, more kinks around the six axial directions, sticking probabilities $P_c>P_m$, and growth rates $V_c>V_m$ (c, corner; m, central part of a face). (b) After crystal has grown out and becomes faceted, the corners are closer to the outer circular source ($r_c<r_m$) $V_c>V_m$ in spite of $P_c>P_m$. (c) Further growth of the crystal leads to a preeminence of dendritic protrusions.

terfacial supersaturation variation on the growth morphology implicitly via the random-walk process. We have only chosen to neglect the influence of the interfacial supersaturation variation on the sticking probability. This assumption is equivalent to that used by Gilmer and Bennema[21] in their calculations of impingement rates. A more realistic description requires more physical input that would, for instance, be obtained from a molecular-dynamics model.

The effect of supersaturation is illustrated in Fig. 5, where β is held constant ($\beta=0.4$ or $\phi_1/kT=0.92$) while γ is varied. At this value of β the crystal can no longer retain a compact form even at low supersaturations [Fig. 5(a)]. Sidebranches appear [Fig. 5(b)] and become more pronounced [Figs. 5(c) and 5(d)] as γ is increased. However, the effect of varying γ is somewhat different from varying β. An increase in γ not only results in more sidebranches but also causes tip splitting.[29]

The dependence of the crystal morphology on the parameters β and γ is tightly coupled. Based on our results, we can draw a more general conclusion which is summarized in Fig. 6. Depending on the value of ϕ_1/kT and $\Delta\mu/kT$, the growing crystal can acquire one of the following morphologies: compact faceted (region I), compact branched and sidebranched (region II), and open multiple sidebranched (dendritic) (region III). In general, the supersaturation ($\Delta\mu$) above which the compact-faceted form is no longer stable decreases with decreasing bond strength (ϕ_1) or increasing temperature. A theoretical study of the roughness of the crystal-melt boundary by Temkin[36] realized that in the parameter space (γ^*,β^*), where β^*, in his case, represents the degree of supercooling and γ^* the bond strength, there are two morphologically distinct regions. The first region corresponds to smooth faceted surfaces, while the second corresponds to a region of "barrierless solid-liquid transition,"[37,38] i.e., atomically rough or nonfaceted surfaces. For the case of a supersaturated nutrient rather than a supercooled melt, the border between regions I and II in our Fig. 6 gives an analogous result. The only difference is that the range of the facets is narrower in our case. The reason is that nutrient diffusion was not taken into account by Temkin. We have found that nutrient diffusion is always a destabilizing factor and reduces the range over which facets can exist.

Our results emphasize a fundamental difference between crystal growth and DLA. The scale invariance exhibited by DLA (Refs. 24 and 39) does not generally hold in (dendritic) crystal growth. In our simulation the instantaneous fractal dimension decreases as the size of the growing crystal increases. From Fig. 7, in which all simulation or growth parameters β, γ and ζ are constant, one can see that a faceted crystal [Fig. 7(a)] can lose its stability as its size increases and exceeds a critical limit [Fig. 7(b)]. This trend is also indicated in the shape evolution of the colored regions in Figs. 3–5. This observation is compatible with previous theories[4,7] of faceted-growth-shape stability.

The above results allow for a microscopic interpretation of the morphological transition exhibited by a growing crystal. The growth (occupation) probability P_{gi} at any perimeter site i of any growth pattern can be decomposed into

$$P_{gi}=(P_{ni}+P_{si})P_i \ , \tag{20}$$

where P_{ni} is the probability that a growth unit has diffused through the nutrient directly to site i, P_{si} is the probability that a growth unit has diffused on the surface to site i (following the arrival at some other surface site through volume diffusion), and P_i is the orientation-dependent sticking probability defined by Eq. (12). For an initially circular nucleus, P_{ni} is a constant, but P_i has maxima along the six axial directions because of the higher kink or dangling-bond density in those higher index planes [see Fig. 8(a)]. Accordingly, the growth rate will be greatest along these six directions. As the crystal grows and develops into a faceted form [Fig. 8(b)], the P_{ni} will no longer be orientation independent. Since the corners are closer to the outer circular source ($r_c<r_m$), or the unscreened opening angle α to accept the incoming molecules is larger,[29] the crystal will gain more particles along these six axial directions, and protrusions will develop [Fig. 8(c)].

There are two mechanisms which counter the destabilizing influence of volume diffusion on faceted morphologies: (a) The redistribution of these local accumulations of growth units through surface diffusion and (b) the tendency of a depression in a face to increase the local sticking probability. Note that in our formulation these effects are coupled. A slight depression will form in a part of the interface (such as the center of a facet) because the local supply rate of growth units through volume diffusion is low. As a consequence energetically favorable sites remain exposed that have a larger number of neighbors than sites on a smooth facet. This increases both the probability that the flux to these sites will be augmented by surface diffusion [Eq. (14)] and the sticking probability P_i [Eq. (12)]. Equation (20) embodies this interplay between volume diffusion and "surface kinetics" (i.e., sticking probability and surface diffusion). A decrease in P_{ni} can be offset by increases in P_{si} and P_i up to some critical value which is determined by the limited range of these local morphology-dependent parameters. When surface kinetics is rate limiting, i.e., for larger bond energy and/or lower temperature, the ability of a faceted crystal to resist the morphologically destabilizing effect of volume diffusion is large.

This interplay is compatible with Chernov's theory of growth-shape preservation for faceted crystals,[4] except that our simulations, and likely also real systems,[40] never exhibit protrusions at face centers. Thus, the predicted equivalence of the effect of protrusions and depressions at face centers[4] cannot be evaluated from these simulations.

The stabilizing effect discussed above is accomplished by the collective effect of P_i, $P_{i\to j}$ or P_{si}. In the work of Vicsek, and Witten and Sander discussed in the Introduction, the aggregate morphologies also exhibited some sensitivity to the nature of the sticking conditions and an attempt was made to directly relate the simulation parameters to the macroscopic Gibbs-Thomson relation.[41] In both cases the notion of a "capillary length" resulted, and

indeed, the effect of this length scale is manifested in the results of their simulations. In particular Witten and Sander found that when viewed on scales in excess of some radius R_{max}, the aggregate had no natural length scale. Furthermore, they found that the value of R_{max} is dependent on the particular form of the sticking conditions employed in the simulations. These findings are compatible with our results. However, we have a different interpretation as to their physical significance. From our simulations the dependence of morphology on the attachment probabilities can be seen as a collective effect of "molecular" interactions occurring at molecular length scales, although the results may be manifested at larger scales (e.g., the existence of macroscopic facets). The difference between our interpretation and the earlier analogies to Gibbs-Thomson effects lies in the physical length scale on which the sticking-probability conditions apply. The scale at which the simulations take place is a molecular length scale.[42] At this level the form that a microscopic counterpart to the Gibbs-Thomson relation should take is not well defined, although it would certainly involve long-range molecular interactions. To anticipate the continuum limit of this crystal-growth problem by applying, at the molecular level, a Gibbs-Thomson-type condition based on an approximation to the local curvature, suppresses the influence of molecular kinetics at the surface. Furthermore, while such an approximation might result in an effect reminiscent of capillary stabilization and favor the growth of more compact objects, short-wavelength noise still exists due to the random behavior of molecules.

V. SUMMARY

The combined effects of nutrient diffusion and surface kinetics on crystal-growth morphology has been considered via a Monte Carlo simulation of growth from a dilute binary gas. A variety of conditions, ranging from kinetic- to diffusion-controlled growth were examined, and successive transitions from compact faceted (dominant surface kinetics) to open dendritic morphologies (dominant volume diffusion) were obtained. While previous simulations, based on DLA-type models, have succeeded in producing dendritic aggregates, the physical basis for the choice of a sticking coefficient in these studies is unclear. Any agreement between a natural phenomenon and a mathematical model lacking a well-defined physical basis is perhaps fortuitous. In order to realize the full potential of such models, we have used simple constitutive relations for surface diffusion and sticking probability based on kinetic considerations. Thus, we are able to interpret what would otherwise be abstract parameters in terms of actual growth conditions. This extension of DLA-type simulations to include a consideration of crystal-growth kinetics affords physical insight into the nature of the interaction between surface and volume processes.

ACKNOWLEDGMENTS

The authors are grateful for the support provided by the Microgravity Science and Applications Division of the National Aeronautics and Space Administration under Grant No. NAG-1-733. We would also like to thank Dr. Mahito Kohmoto for introducing R. F. X. to Monte Carlo simulation and the basic ideas of diffusion-limited-aggregation models. Stimulating discussions with Professor I. Sunagawa are also very much appreciated.

[1]F. C. Frank, in *Growth and Perfection of Crystals,* edited by R. H. Doremus, B. W. Roberts and D. Turnbull (Wiley, New York, 1958), p. 3.
[2]A. Seeger, Philos. Mag. **44**, 1 (1953).
[3]J. W. Cahn, in *Proceedings of the International Conference on Crystal Growth, Boston, 1966,* edited by H. S. Peiser (Pergamon, Oxford, 1967), p. 681.
[4]A. A. Chernov, J. Cryst. Growth **24/25**, 11 (1974).
[5]S. R. Coriell and R. F. Sekerka, J. Cryst. Growth **34**, 157 (1976).
[6]T. Kuroda, T. Irisawa, and A. Ookawa, J. Cryst. Growth **42**, 41 (1977).
[7]C. Kumar and J. Estrin, J. Cryst. Growth **51**, 323 (1981).
[8]A. A. Chernov, in *Modern Crystallography III,* Vol. 36 of *Springer Series in Solid State Sciences,* edited by M. Cardona, P. Fulde, and H.-J. Queisser (Springer-Verlag, Berlin, 1984).
[9]P. Curie, Bull. Soc. Min. France **8**, 145 (1885).
[10]G. Wulff, Z. Kristallogr. Mineral. **34**, 449 (1901).
[11]I. N. Stranski and R. Kaischew, Z. Kristallogr. Mineral. **78**, 373 (1931).
[12]C. Herring, in *Structure and Properties of Solid Surfaces,* edited by R. Gomer and C. S. Smith (University of Chicago Press, Chicago, 1953), p. 5.
[13]R. Lacmann, Neues Jahrb. Mineral. **122**, 36 (1974).
[14]M. Wortis, in *Chemistry and Physics of Solid Surfaces,* edited by R. Vaneslow (Springer-Verlag, Berlin, in press), Vol. VII.
[15]R. L. Parker, in *Solid State Physics,* edited by H. Ehrenreich, F. Seitz, and D. Turnbull, (Academic, New York, 1970), Vol. 25, p. 151, and references therein.
[16]J. S. Langer, Rev. Mod. Phys. **52**, 1 (1980).
[17]N. Metropolis, A. W. Rosenbluth, M. N. Rosenbluth, A. H. Teller, and E. Teller, J. Chem. Phys. **21**, 1087 (1953).
[18]A. A. Chernov and J. Lewis, J. Phys. Chem. Solids **28**, 2185 (1967).
[19]H. Müller-Krumbhaar, in *Monte Carlo Methods in Statistical Physics,* edited by K. Binder (Springer-Verlag, Berlin, 1979), p. 295, and references therein.
[20]F. F. Abraham, Adv. Phys. **35**, 1 (1986).
[21]G. H. Gilmer and P. Bennema, J. Appl. Phys. **43**, 1347 (1972).
[22]W. W. Mullins and R. F. Sekerka, J. Appl. Phys. **35**, 444 (1964).
[23]T. A. Witten and L. M. Sander, Phys. Rev. Lett. **47**, 1400 (1981).
[24]T. A. Witten and L. M. Sander, Phys. Rev. B **27**, 5686 (1983).
[25]J. R. Banavar, M. Kohmoto, and J. Roberts, Phys. Rev. A **33**, 2065 (1986).

[26]T. Vicsek, Phys. Rev. Lett. **53**, 2281 (1984).
[27]T. Vicsek, Phys. Rev. A **32**, 3084 (1985).
[28]C. Tang, Phys. Rev. A **31**, 1977 (1985).
[29]J. Nittmann and H. E. Stanley, Nature **321**, 663 (1986), and references therein.
[30]R. C. Ball, Physica A **140**, 62 (1986).
[31]F. Rosenberger, in *Interfacial Aspects of Phase Transformations,* edited by B. Mutaftchiev (Reidel, Dordrecht, 1982), p. 315.
[32]J. Nittmann, G. Daccord, and H. E. Stanley, Nature **314**, 141 (1985).
[33]C. C. Lin and L. A. Segel, *Mathematics Applied to Deterministic Problems in the Natural Sciences* (Macmillan, New York, 1974).
[34]T. L. Hill, *An Introduction to Statistical Thermodynamics* (Dover, New York, 1986), p. 79.
[35]P. Meakin, Phys. Rev. A **33**, 3371 (1986).
[36]D. E. Temkin, in *Crystallization Processes,* edited by N. N. Sito (Consultants Bureau, New York, 1969), p. 15.
[37]J. W. Cahn, Acta Metall. **8**, 554 (1960).
[38]A. L. Roitburd, Kristallografiya **2**, 292 (1962).
[39]H. E. Stanley, in *On Growth and Form,* edited by H. E. Stanley and N. Ostrowsky (Nijhoff, Dordrecht, 1986), p. 21, and references therein.
[40]I. Sunagawa (private communications).
[41]While the term "Gibbs-Thomson" commonly refers to an equation for the local correction to the bulk equilibrium melting temperature due to the curvature of the solid surface, we shall use it in the more general sense to refer to the local change in chemical potential due to the surface curvature.
[42]Our sticking conditions are, in accord with the physical basis between random walks and diffusion, based on molecular kinetics considerations which we further limit to nearest- and next-nearest-neighbor interaction. Thus for our simulations the sticking probability is related only to a very local configuration of the surface at molecular scales.

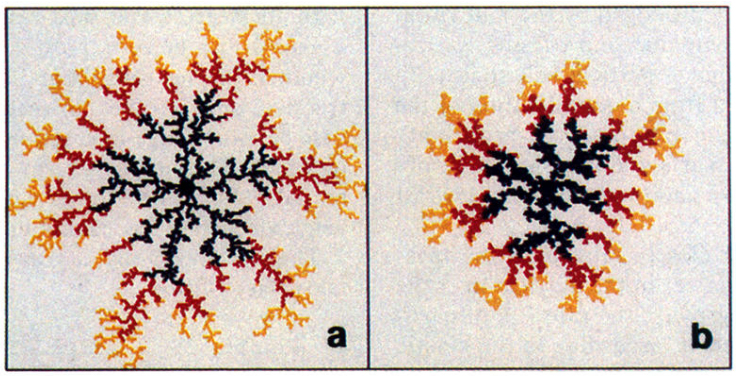

FIG. 1. Results of DLA on a 2D triangular lattice for 3×10^3 growth units. The colors represent time sequences of the growth patterns. (a) Sticking coefficient $t=1$; (b) sticking coefficient $t=0.6$.

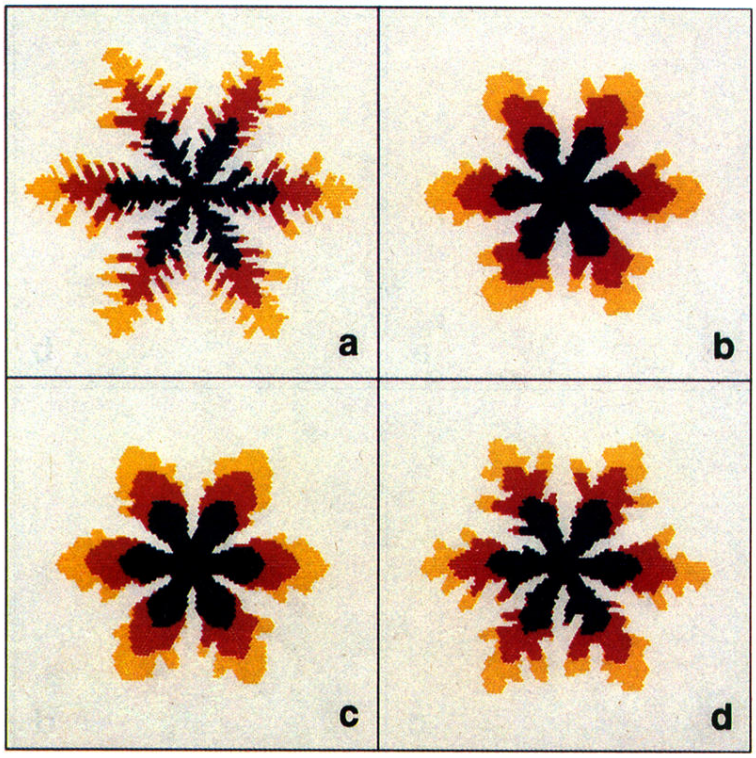

FIG. 3. Effect of surface diffusion and next-nearest-neighbor interaction on growth pattern at constant $\gamma=2$ or $\Delta\mu/kT=0.69$, and $\beta=0.6$ or $\phi_1/kT=0.51$, for 3×10^3 growth units. (a) Without surface diffusion and $\zeta=0.0$; (b) with surface diffusion and $\zeta=0.0$; (c) with surface diffusion and $\zeta=0.1$; (d) with surface diffusion and $\zeta=-0.1$.

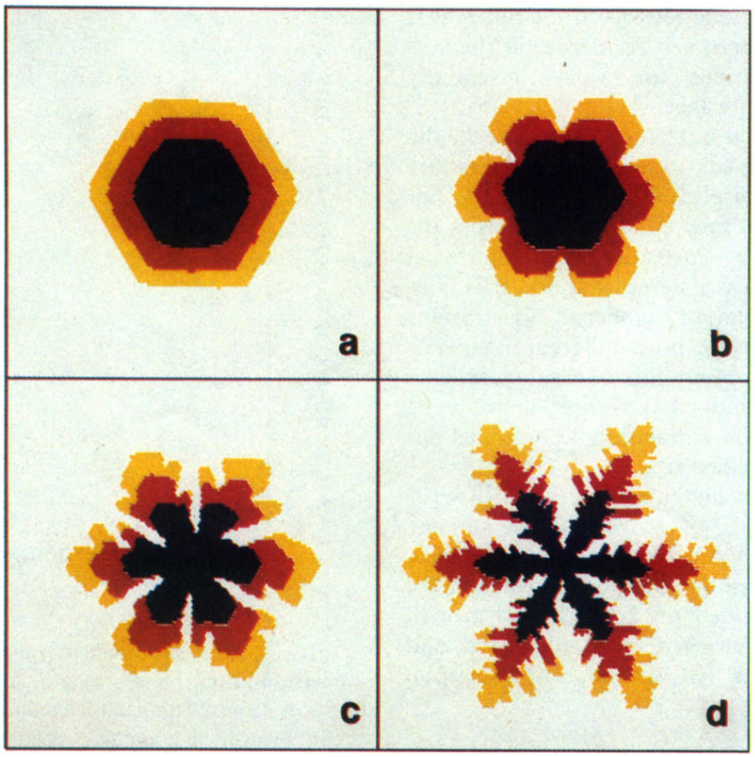

FIG. 4. Effect of bond strength and temperature on growth patterns of a crystal with surface diffusion at $\gamma=2$ or $\Delta\mu/kT=0.69$ and $\zeta=0.0$. (a) $\beta=0.02$ or $\phi_1/kT=3.91$; (b) $\beta=0.1$ or $\phi_1/kT=2.30$; (c) $\beta=0.5$ or $\phi_1/kT=0.69$; (d) $\beta=0.7$ or $\phi_1/kT=0.36$.

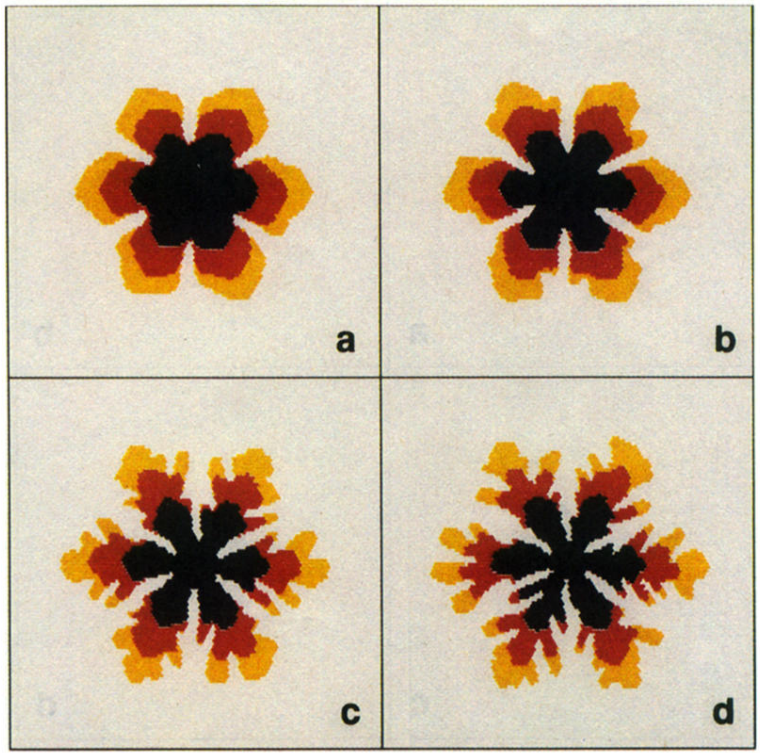

FIG. 5. Effect of supersaturation on growth patterns of a crystal with surface diffusion at $\beta=0.4$ or $\phi_1/kT=0.92$ and $\zeta=0.0$. (a) $\gamma=1.2$ or $\Delta\mu/kT=0.18$; (b) $\gamma=2.0$ or $\Delta\mu/kT=0.69$; (c) $\gamma=5.0$ or $\Delta\mu/kT=1.61$; (d) $\gamma=10.0$ or $\Delta\mu/kT=2.3$.

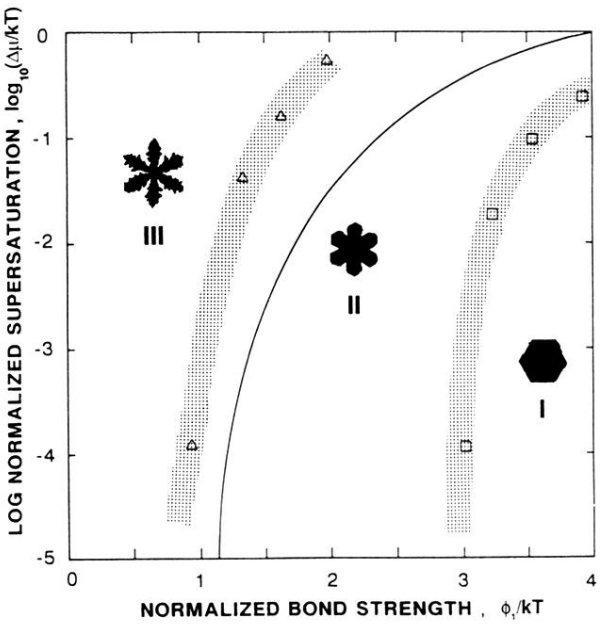

FIG. 6. Crystal-growth morphology as a collective effect of supersaturation, bond strength, and temperature. In region I crystals acquire compact-faceted forms; in region II crystals become protruded branchless needles with sixfold symmetry; in region III crystals become dendrites with multiple sidebranches. Symbols: Monte Carlo results judged as "boundary cases." Solid line: Temkin's (Ref. 36) boundary between faceted and nonfaceted growth for a simple cubic lattice.

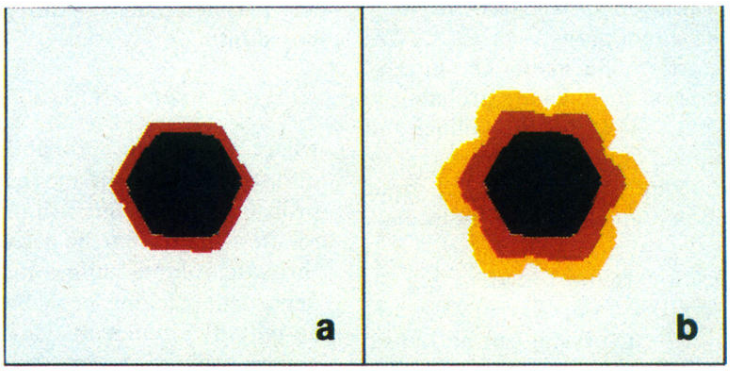

FIG. 7. Crystal size dependence of morphological stability, $\gamma = 1.2$, $\beta = 0.1$, $\zeta = 0.1$, and with surface diffusion. (a) Crystal of 1.5×10^3 particles is still faceted; (b) facets on crystal of 3×10^3 particles lose their shape stability.